COMMUNICATION

Check for updates

Learning and spiking dynamics in brain-like nanoscale networks†

B. L. Monaghan, [iD]ᵃ Z. E. Heywood, [iD]ᵃ S. J. Studholme, [iD]ᵃ F. Houard, [iD]ᵇ J. Grisolia, [iD]ᵇ S. Tricard [iD]ᵇ and S. A. Brown [iD]*ᵃ

Neuromorphic approaches to computation are driven by both the low-power operation of the biological brain and ever-increasing energy consumption of modern computing systems. Percolating networks of nanoparticles are promising candidates for self-assembled neuromorphic hardware systems as they exhibit a range of brain-like properties, including neuron-like spiking dynamics and critical behaviour. Here we show that random placement of synaptic memristors within these neuron-like networks leads to changes in the spiking dynamics and to learning behaviour. We consider two models of the memristors and show that different types of memristive hysteresis lead to differing effects on the network-level spiking dynamics. We then demonstrate that mixtures of neurons and synapses exhibit potentiation and de-potentiation, *i.e.* learning and forgetting. These results suggest that the addition of synaptic 'memory' to self-assembled networks provides functionality that could enable new types of computation.

New concepts

Percolating networks of nanoparticles exhibit brain-like properties and so are promising candidates for fabrication of self-assembled nanoscale hardware variants of neural networks. However, to date, the absence of intrinsic memory has meant that learning must be performed outside the networks. Here we replace a portion of the "spiking neurons" in the networks with memristive "synapses", and demonstrate biologically realistic potentiation behaviour *i.e.* learning. More specifically we show that different memristor properties lead to learning behaviour on different timescales and to different neural spiking dynamics in the networks. This work therefore provides a key step towards building more realistically brain-like nanoscale networks, to incorporating synaptic functionality, and towards enabling new types of neuromorphic computation with self-assembled networks.

1 Introduction

As global demand for high-performance computing systems increases, the scale and performance limits of conventional transistor-based architectures have become increasingly apparent, and concerns about the energy consumption of these systems have grown. In response, alternative ('neuromorphic') approaches to computation inspired by the human brain have been proposed to mitigate and overcome these issues.[1,2] The brain is a very high-performance cognitive system that operates with remarkable energy efficiency,[3] and so the development of computers that take inspiration from the brain could provide powerful and energy efficient new information processing systems.

Self-assembled nanoscale systems such as networks of nanowires and nanoparticles are promising for neuromorphic computing due to their small scale, inherent brain-like properties, and low power consumption.[4,5] In both nanowire networks (NWNs)[6–10] and percolating networks of nanoparticles (PNNs)[11–17] brain-like dynamics emerge from the complex collective response of the junctions between the nanowires or nanoparticles. We focus here on PNNs because – as will be

ᵃ *The MacDiarmid Institute for Advanced Materials and Nanotechnology, School of Physical and Chemical Sciences, University of Canterbury, Christchurch, New Zealand. E-mail: simon.brown@canterbury.ac.nz*

ᵇ *Laboratoire de Physique et Chimie des Nano-Objets, INSA, CNRS, Université de Toulouse, 135, av de Rangueil, 31077 Toulouse Cedex 4, France*

† Electronic supplementary information (ESI) available. See DOI: https://doi.org/10.1039/d5nh00407a

We are very pleased to publish this, our third article in Nanoscale Horizons, as part of the 10th anniversary issue. It describes new simulations that capture the potential for nanoscale memristors to be added self-assembled devices in order to modify performance and as the basis for new applications. I have appreciated the very reasonable and thoughtful approach taken by the Editors at this journal and I hope that we will continue to publish here.
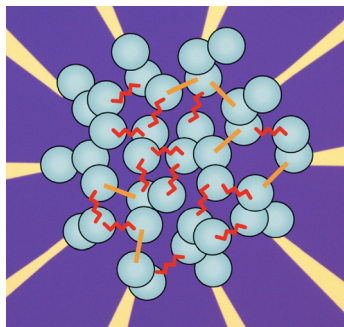
S. A. Brown

Fig. 1 Schematic of a PNN showing groups of nanoparticles (pale blue), spiking tunnel gaps (red), and introduced memristors (orange). In this example 30% of the original tunnel gaps have been replaced by memristors.

explained below – they are remarkably robust and can be operated in a regime where information is processed through neuron-like spikes, as in the brain. Spiking is believed to provide significant computational advantages, such as low power consumption and suitability for tasks that require processing of temporal information, *e.g.* real-time decision-making.[18]

1.1 Percolating networks of nanoparticles

PNNs exhibit small-world and scale-free topologies, stochastic spiking, and brain-like dynamics with long-range temporal correlations.[19–22] As shown schematically in Fig. 1, PNNs are comprised of metallic nanoparticles deposited onto an atomically smooth insulating substrate. Particles are deposited until the surface coverage p reaches the percolation threshold ($p_c \sim$ 0.68 for 2D continuum percolation[23]). In this regime the conductance of the PNNs is dominated by tunnel gaps between highly conducting groups of nanoparticles (Fig. 1).

When a voltage V_{app} is applied to the input electrodes, electric field-driven surface diffusion processes[11] cause atoms to migrate within the tunnel gaps. Fig. 2a and b show the initial growth at *low* voltages of a 'hillock' within a tunnel gap. The hillock decreases the tunnelling distance and hence increases the conductance of the gap (if V_{app} is decreased surface energy effects cause the decay of the hillock, decreasing the conductance). These dynamics have been shown to lead to memristive behaviour[24] (see discussion of synapses below) and allow implementation of neuromorphic computational schemes such

as reservoir computing[25–28] (note that related computations have been performed with NWNs[7–9]), in addition to computation schemes based on neuron-like spiking.[29,30]

Fig. 2c shows that *high* voltages lead to formation of atomic-scale filaments that bridge the tunnel gap, causing a sudden increase in conductance. The filaments later break due to electromigration effects.[11] The formation and destruction of these filaments generates neuron-like spiking events,[19] and it has been shown that the atomic-scale dynamics resemble leaky integrate-and-fire behaviour in biological neurons.[20] Together with the scale-free topology of the PNNs,[12,21] these dynamics result in highly correlated scale-invariant bursts of network activity – 'avalanches' – that are quantitatively similar to those in the human brain. The avalanches meet strict criteria for criticality[19] which is associated with optimum computation and is thought to be the operating point of the brain.[31,32] Several types of computation have been successfully demonstrated that exploit this spiking,[29,33] but exploitation of criticality for specific tasks is a remaining challenge.[30]

Experimental fabrication of PNNs has been described in detail in ref. 12. The physical devices are remarkably robust and can be easily integrated with CMOS electronics, making them attractive for real-world applications.[26] Physically realistic simulations of both the electrical and neuromorphic properties of PNNs have previously been shown to be in excellent agreement with experimental results,[20] confirming that a model of percolation with tunnelling[34] provides an accurate description of the real physical system. We highlight that simulations include a model of neuron-like spiking based on the formation and breaking of atomic-scale filaments (see Methods, eqn (2) and (3)). Here we label this the 'Type A' model, in anticipation of the models of memristive/synaptic behaviour that will be introduced below.

1.2 The need for synaptic plasticity

A key feature of the biological brain is the connectivity between neurons, which is provided by synapses. Modulation of synaptic connections is a key mechanism for the formation and storage of memory.[35] In PNNs, the (volatile) memristive behaviour in the low voltage regime provides short term memory but in the high voltage spiking regime there is no synaptic/memory mechanism: the connectivity of the network of neurons is fixed and learning must be performed outside the network.[29] Incorporation of synapses within these spiking neural networks would be a significant step towards the construction of more biologically-realistic self-assembled systems, as well as possibly allowing tuning of the networks between critical and non-critical states and enabling a range of different computational algorithms to be implemented. Learning is a key kind of neuromorphic behaviour that is necessary for a range of applications, including associative learning,[36] unsupervised learning,[37] and reservoir computing,[26–28] and has been especially emphasised in the literature on related nanowire devices.[7,38,39]

Fig. 1 shows schematically the replacement of some spiking tunnel gaps (red) with new memristive elements (orange). We expect that such memristive synapses can be incorporated into PNNs experimentally by methods such as deposition of inorganic coating materials,[40] by controlled sulphidisation of Ag or Cu
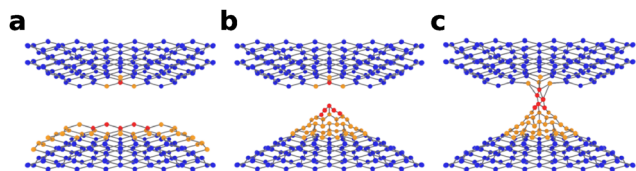

Fig. 2 Hillock and filament formation in PNNs. (a) A schematic of a tunnel gap that separates two nanoparticles prior to the formation of a hillock. (b) In response to an applied network voltage, the electric field in the gap forms a hillock which decreases the size of the tunnel gap and increases its conductance. Hillock growth (relaxation) is driven by the electric field (surface tension).[24,25] (c) After a sufficiently long time, or at sufficiently large applied voltages, an atomic-scale filament forms that fully bridges the tunnel gap. Electromigration later leads to breaking of the filament.

PNNs,[6,41] or by the introduction of novel memristive molecules.[42–44] First steps in this direction were taken in ref. 45, although we note the network architecture in that case is different to that of the PNNs considered here.

Here we show, using physically realistic simulations, that the addition of memristive synapses to PNNs controls the connectivity between neuron-like tunnel gaps and significantly modifies the network properties. We begin by considering two different models of memristive synapses and show that different parameterisations in the models lead to very different hysteresis of the *individual* memristors, which in turn lead to different hysteresis in the *networks*. We then show that when the individual memristor characteristics are tuned appropriately the inclusion of 'synapses' in the networks significantly changes the spiking dynamics (*e.g.* patterns of long range temporal correlations). We further demonstrate that the mixed networks exhibit clear learning behaviour: in response to sequences of voltage pulses the plasticity of the synapses leads to increases in network conductance, increased connectivity between neurons, and hence to increased neuronal spiking. In the absence of stimulus the synapses de-potentiate, and the network conductance and spike rate both decrease. Both learning *and* forgetting[46] are essential for various types of brain-like computation (see ref. 30, 37 and 47–49 and references therein). We emphasise that the results presented here are from simulations, but that they pave the way for new experiments which we hope to report on in the near future.

2 Results

The focus of this paper is on the changes in *network* dynamics that result from the introduction of memristive synapses. We begin by discussing the dynamics of the *individual* memristors

and showing the effects of incorporating new memristors into the networks in the low voltage regime (*i.e.* in the absence of spiking). We then demonstrate their effects on the spiking dynamics in the high-voltage regime, where the behaviour of the memristors complements that of the spiking tunnel gaps. Lastly, we demonstrate the network plasticity that results from inclusion of memristors with appropriately chosen parameters.

2.1 Memristor models

Two memristor models were investigated to complement the spiking tunnel gaps governed by the Type A model discussed above. The first is a model that has previously been used to simulate memristive tunnel gaps in PNNs (*i.e.* the formation of hillocks, as in Fig. 2) in the low-voltage regime.[24,25] It models atomic-scale dynamics that are linear in response to the local gap voltage V_g. We label this model 'Type B', and it is governed by eqn (4) and (5) (see Section 5.3).

The second memristor model was developed to capture electrochemical effects in memristive junctions between Ag NWNs.[8,39] This model is governed by eqn (7)–(10) (see Section 5.4). This 'Type C' model provides greater ability to precisely tune the size and shape of memristive hysteresis loops due to its large parameter space and its exponential dependence on the local voltage.[50] Note that both models describe volatile memristors since this allows for 'forgetting' (see Section 2.6). Both models are unipolar to maintain consistency with previous work.[8,20]

We emphasise that the Type B model is derived from the Type A model, whilst the Type C model is an entirely separate model that was developed as a way of modelling very different memristive devices. The Type B model is similar to the Type A model in the low voltage regime, where only continuous changes of the gap resistance is allowed. The main difference is that at high voltages the Type A model generates
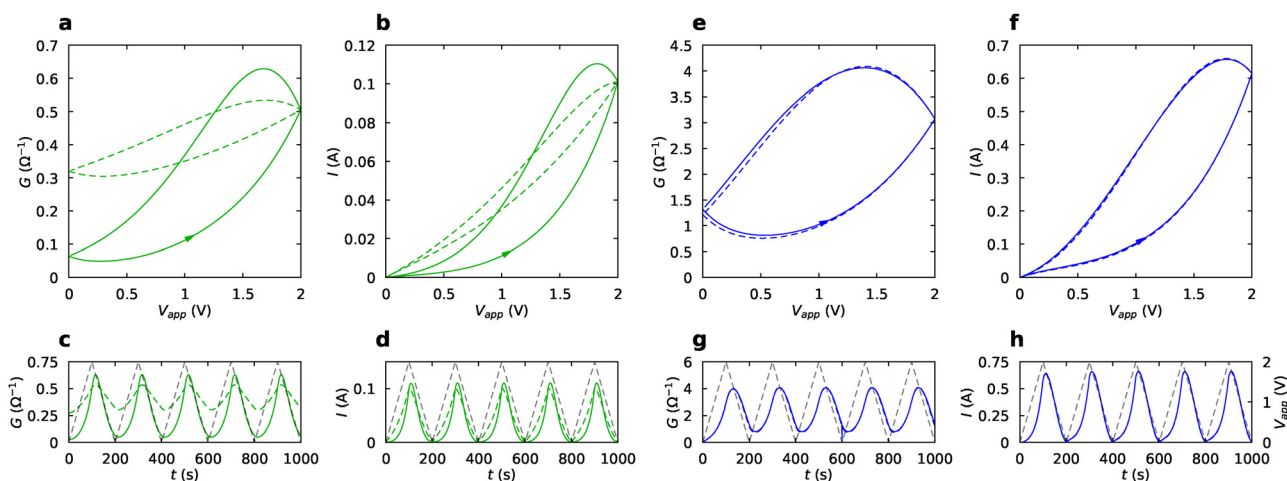

Fig. 3 Hysteresis of single memristors and networks of memristors (dashed and solid lines respectively). Green and blue curves are for Type B and Type C memristor cases. The hysteresis is shown in several forms: (a) and (e) $G–V$ curves. (b) and (f) $I–V$ curves. (c) and (g) $G–t$ trace. (d) and (h) $I–t$ trace. In general, plotting conductance enhances the visibility of the hysteresis. The voltage ramps (grey dashed lines) have $V_{max} = 2$ V for the network of 100% memristors (panels (c), (d), (g) and (h)) and $V_{max} = 0.2$ V for the single memristors. $V_{min} = 0$ V, period = 200 timesteps. The conductance and current of the single memristors are scaled such that the values at the peak voltage are equal to those of the 100% networks to clearly show the hysteresis (this results in the dashed and solid lines being almost identical in panels (e)–(h)).

discontinuous changes in resistance *i.e.* spikes. This spiking is the result of filament formation and breaking in "virgin" nanogaps between nanoparticles whereas memristive behaviour is a property of additional memristors (*e.g.* molecules or sulphides).

This paper discusses the effect of replacing (randomly chosen) Type A tunnel gaps with Type B or C memristors. We label the networks according to the type of memristor and the ratio: for example, an 'A : C = 75 : 25 network' refers to one in which 25% of its tunnel gaps were replaced with Type C memristors. Section S1 (ESI†) discusses the effects of different parameter choices in each model. In particular, Section S1.4 (ESI†) shows that the relative conductances of the gaps/memristors does not have a significant impact on the observed network properties.

2.2 Hysteresis of single memristors and networks of memristors

Memristors are typically characterised by performing current–voltage (I–V) measurements, and the observed hysteresis loops are signatures of both non-linear and memory effects. Plotting the data as conductance–voltage (G–V) curves can be useful in clarifying the amount of hysteresis in some cases.

Fig. 3 compares the hysteresis of single Type B and C memristors (dashed lines) with the hysteresis of 100% memristor networks (solid lines). G–V and I–V curves are shown in panels (a), (e) and (b), (f) respectively. Note that the voltage applied to the individual memristors V is 10 times lower, because in the networks the applied voltage V_{app} is dropped across approximately 10 gaps in series. The conductance and current of the single memristors are normalised to be equal to those of the 100% networks at V_{max}.

Fig. 3a–d show that for the Type B memristors there is a significant difference in the shape of the hysteresis for a single memristor and a network of memristors. The difference is due to the heterogeneity of the Type B memristors (the conductance of each memristor depends on the length of the tunnel gap within which it is located; see eqn (5)). In contrast, Fig. 3e–h show that the hysteresis measured for a single Type C memristor is very similar to that of the network (Type C memristors are homogeneous, with identical parameters). Networks containing a *mixture* of Type A gaps and Type B/C memristors exhibit hysteresis that is similar to that of the 100% memristor networks (Fig. S2 (ESI†)), as long as the applied voltage is small enough to avoid spiking. Note that the network currents are orders of magnitude higher than those measured in experiments[11] because the simulation parameters were chosen for consistency with ref. 20 and 22. Simulated currents could be scaled to be more realistic but we choose to maintain consistency with previous work, as this scaling does not impact the results. See Methods (Section 5.2) for more detail.

Section S2 (ESI†) discusses how the applied voltage is distributed in the network. Since the network is complex, scale-free and heterogeneous (comprising tunnel gaps, filaments and memristors) there is a broad distribution of the resultant voltages V_g measured across individual memristors. This in turn leads to a wide range of hysteresis curves for individual memristors, and contributes to the complex dynamics that emerge within the networks.

2.3 Network topology, voltage and current distributions

Fig. 4 compares the network topology, voltage, and current distributions for a 100% Type A gap network (left column), an A : B = 75 : 25 network (middle column), and an A : C = 75 : 25 network (right column). Graph representations of each network are shown in Fig. 4a–c. Each filled circle represents the geometric centre of a group of particles and the links between the nodes (called 'edges') represent the tunnel gaps between each group. Note that the tunnel gaps into which new memristors are inserted are the same in panels (b) and (c): the nodes and edges are unchanged, but the *type* of edge changes.

Fig. 4d–f and g–i show the voltages at each group of nanoparticles and the currents through each tunnel gap respectively. In panels (d)–(f) the nanoparticle groups are coloured by their potential to ground, and in panels (g)–(i) the tunnel gaps (including both Type A gaps and memristors) are coloured by the magnitude of their current flow. The maps of voltages and currents are similar for all three cases showing that the inclusion of memristors does not significantly alter the network topology.

Section S3 (ESI†) discusses in detail the differences between networks containing Type B and Type C memristors, and in particular compares in detail the distributions of the voltages across each memristor and their conductances. The voltage distributions for networks with Type B memristors are shown to more closely follow power law distributions, consistent with critical dynamics. It is shown that this is at least partially because the range of conductances of the Type B memristors is larger than for the Type C memristors, and consequently that the distributions of voltages and currents in the networks with Type C memristors are more uniform.

2.4 Spiking dynamics

Fig. 5 compares the output currents for networks containing Type B and C memristors with those for a 100% Type A gap network. In Fig. 5a and b, the spiking in the network of Type A gaps is characterised by avalanches of spiking events,[19] with a low baseline current. Each change in the current corresponds to formation or breaking of an atomic scale filament. In Fig. 5c and d, the spiking behaviour can still be observed in the A : B = 75 : 25 network but the inclusion of Type B memristors leads to some continuous changes in current (panel (d)) and to subtle differences in the spiking patterns (discussed in Section 2.5). The baseline current is higher (when the voltage is applied the conductance of the individual memristors increases, causing an increase in the network conductance) and the sizes of the spikes are generally smaller than those in panels (a) and (b). In Fig. 5e and f the spiking activity of the A : C = 75 : 25 network is again subtly different, and in panel (f) the continuous conductance changes of the Type C memristors are even more evident. A further increase in the base conductance can also be observed, and the size of the spikes is again smaller, as the average conductance of the Type C memristors is higher.
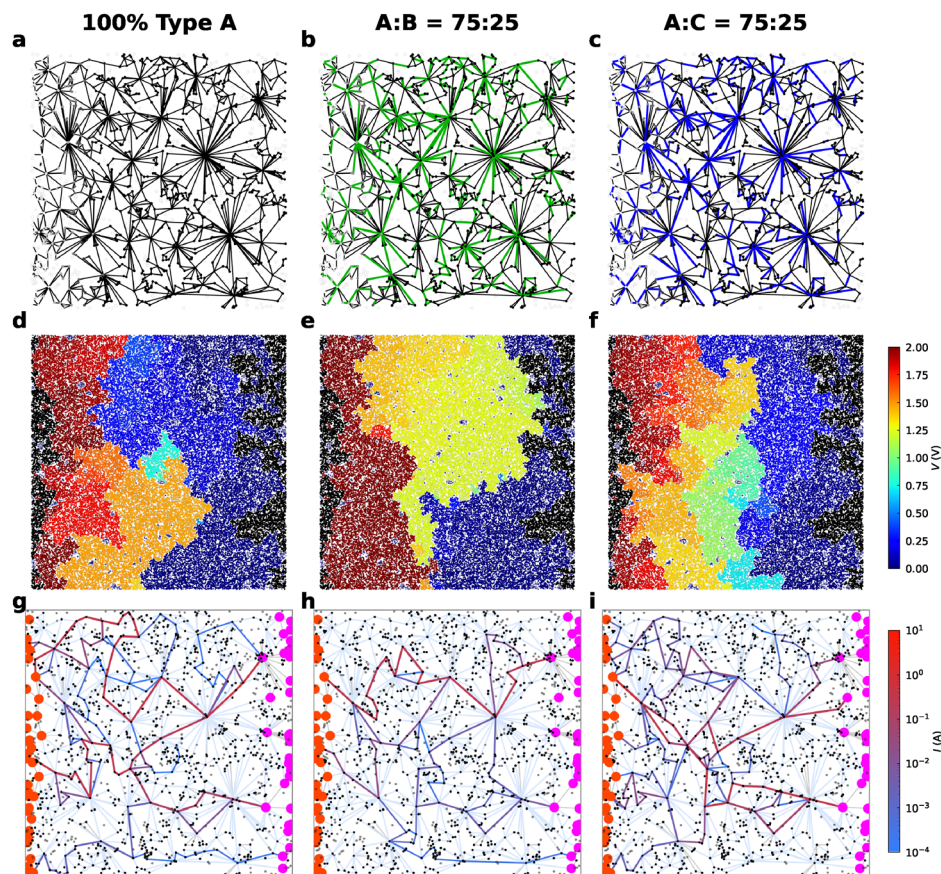
Fig. 4 Physical characteristics of simulated PNNs. 100% Type A gap network (left column), A : B = 75 : 25 network (middle column), A : C = 75 : 25 network (right column). (a)−(c) Graph representations. Nodes represent the geometric centres of the nanoparticle groups while edges represent the tunnel gaps between groups. Type B (Type C) memristors are indicated by green (blue) edges; note that for clarity the coloured edges are slightly thicker than the black edges, which may give the impression that there are more than 25% memristors. (d)−(f) Voltage distribution across the PNNs shown in (a)−(c). A DC bias is applied to the left side of the networks while the right side is held at ground potential. Particles are represented by discs which overlap to form groups, and the colours represent the potential on the groups (relative to ground). Groups that are connected to the electrodes are coloured black. (g)−(i) Current maps for the networks shown in (a)−(c). Note that the pale blue lines represent tunnel gaps carrying no current. Here the input and output electrodes are orange and pink respectively. (d)−(i) are representative snapshots of each network at timestep 500 000. V_{app} = 2 V for all panels.

The key point is that avalanches of spikes are observed in Fig. 5 in all cases, *i.e.* the spiking dynamics are not fundamentally changed by replacing 25% of the tunnel gaps by memristors. The next sections describe the changes in dynamics in more detail.

2.5 Temporal correlations

Temporal correlations in the measured spike trains are typically characterised by examining distributions of inter-event intervals (IEIs) and autocorrelation functions (ACFs).[19,20] Fig. 6a–c compare the IEI distributions for a 100% Type A gap network (red), an A : B = 75 : 25 network (green) and an A : C = 75 : 25 network (blue). Fig. 6d–f show the corresponding ACFs.

In Fig. 6a and b, the power law fits to the tails of the IEI distributions indicate that the critical dynamics previously reported[19,20] in networks of Type A gaps persist after the addition of Type B memristors. However in Fig. 6c, the long-range temporal correlations appear to be more strongly impacted by the presence of Type C memristors, as the range of IEIs is narrower than that in panel (b).

Fig. 6d–f show that long range temporal correlations persist when memristive synapses are added to PNNs. The ACFs are approximately power laws in all cases but the slopes depend on details such as the homogeneity and relative conductances of the memristors in each model – see Section S1 (ESI†). It is likely that the memristive synapses tune the networks away from criticality, but a detailed investigation would be required to confirm this. Such an investigation would require very long simulations and a careful consideration of the possibility of emerging concepts such as quasi-criticality.[51]

2.6 Potentiation and de-potentiation

Persistent changes in synaptic strength that result from stimuli (or absence thereof) are called potentiation and de-potentiation, and are thought to help facilitate the formation of memory in the brain.[35,52] The insertion of memristors into PNNs is intended to provide synaptic plasticity in the form of continuous changes in the conductance of the connections between groups of nanoparticles.
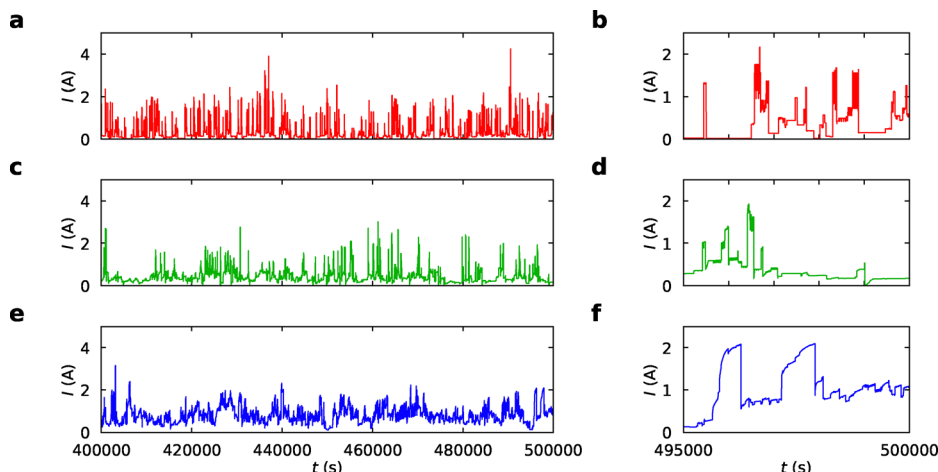
Fig. 5 PNN spiking activity for DC applied voltages. (a) and (b) 100% Type A network. (c) and (d) A : B = 75 : 25 network. (e) and (f) A : C = 75 : 25 network. The left column shows the final 100 000 timesteps of the simulation, while the right column shows the last 5000 timesteps of the same simulation to better show the spiking. Clearly, the spiking dynamics differ significantly between each case. The 100% Type A network shown in (a) and (b) is dominated by large spiking events that decay quickly, while the networks with included memristors shown in (c)–(f) have smaller spiking events that are complemented by continuous changes in the current. Note that V_{app} in panels (c)–(f) is higher (3 V compared to 2 V in panels (a) and (b)) to obtain comparable spiking rates (this is required because some Type A gaps have been replaced by memristors). Note that the current scales observed in panels (c)–(f) are much higher than those in panels (b) and (f) of Fig. 3. This is due to the presence of spiking Type A gaps in the networks depicted in this figure, which yield very high conductances ($\sim 10 \; \Omega^{-1}$) during a spike. We emphasise that the base currents seen in panels (c)–(f) correspond well to the current values observed in Fig. 3.

The relatively small sizes of the networks (200 × 200) discussed in the preceding sections lead to strong stochastic effects (since in some cases there are just a few memristors on the dominant current paths between the electrodes). Hence in this section we focus on larger networks (*i.e.* 800 × 800) where stochastic effects are less dominant. Results for 200 × 200 networks are provided in Sections S4.2 and S4.3 (ESI†) for comparison. The Type A parameters were tuned for the larger network size in order to facilitate comparison with smaller networks (see Section 5.2 for detail).
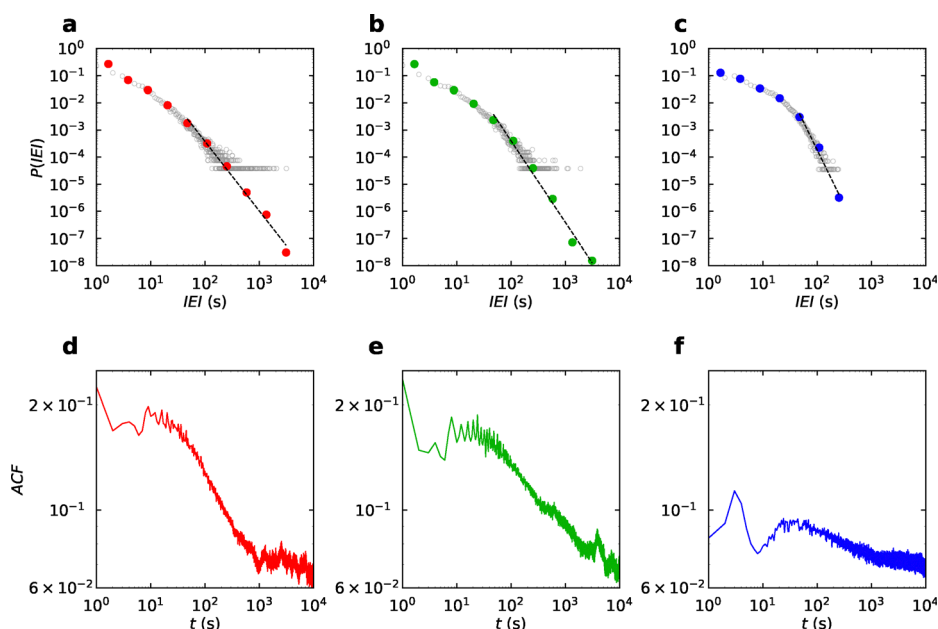

Fig. 6 Inter-event intervals (IEIs) and autocorrelation functions (ACFs). (a)–(c) IEI distributions (PDFs) for a 100% Type A network, an A : B = 75 : 25 network and an A : C = 75 : 25 network. P(IEI) is the probability density for the distributions. (d)–(f) Corresponding ACFs. PDFs calculated with linear (log) bin sizes are plotted as grey (coloured) points. Fits to the IEI distributions are shown as black dashed lines. The data in all panels are obtained from the final 400 000 timesteps of a 500 000 timestep simulation. Note that V_{app} is higher in panels (b, c, e, f) (3 V compared to 2 V in panels (a) and (d)) to obtain comparable spiking rates in the networks with included memristors.
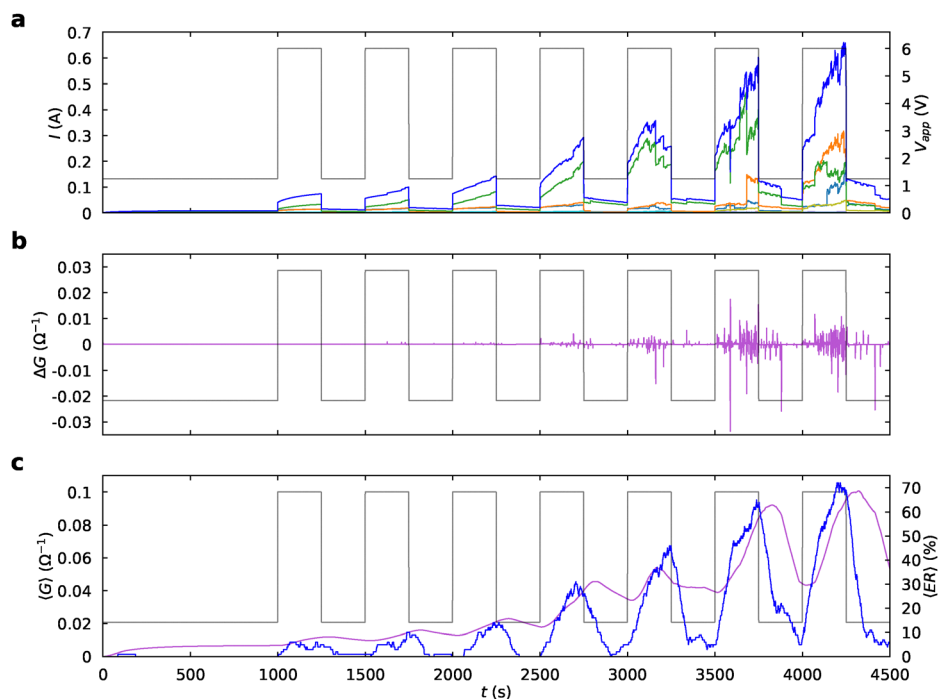
Fig. 7 Demonstration of potentiation effects for an A : C = 75 : 25 network. (a) The total output current (blue) and output currents from individual groups (other colours) as a function of time. The applied voltage V_{app} (V_{min} = 1.25 V, V_{max} = 6 V, pulse length = pulse spacing = 250 timesteps) is plotted in grey in all panels. (b) The corresponding changes in conductance ΔG, showing that amplitude and frequency of spikes increases for successive input pulses. (c) Moving averages (over 100 timesteps) of the network conductance ($\langle G \rangle$, purple) and network event rate ($\langle ER \rangle$, blue).

Fig. 7 shows the response of an A : C = 75 : 25 network to a sequence of seven voltage pulses. Fig. 7a shows the total current (blue curve) as well as the current measured at each electrode (other colours): clearly with each subsequent pulse, the currents increase and there is more spiking activity (see Fig. 7b). These effects are demonstrated even more clearly in Fig. 7c by the moving averages of the conductance ($\langle G \rangle$, purple) and event rate ($\langle ER \rangle$, blue). The increasing network activity in response to a series of voltage pulses is an example of potentiation, which indicates that the Type C memristors perform a synaptic role within the network and allow for the network to 'learn'.

The volatility of the memristors (see Section 2.1) also allows for the networks to 'forget'. Fig. 7c shows a decay in both $\langle G \rangle$ and $\langle ER \rangle$ in the absence of stimulus, i.e. de-potentiation. Fig. S18 (ESI†) shows that if the spacing between stimuli is larger, the memristors de-potentiate further so that the response to subsequent pulses is lowered (smaller increases in $\langle G \rangle$ and $\langle ER \rangle$). Similar potentiation and de-potentiation is also observed in PNNs with Type B memristors, as shown in Fig. S15 and S16 (ESI†). The details of the potentiation and de-potentiation processes depend on specific attributes of the networks and memristor models, but Section S4 (ESI†) shows that qualitatively similar behaviour is observed for a range of parameters.

A range of simulation parameters were tuned to provide the memory observed in Fig. 7, including the size of the PNN, the number and configuration of the input and output electrodes, the ratio of Type A gaps to Type C memristors, and the distribution of the memristors in the network. The characteristics of the applied voltage pulses – including the number, their size (i.e.

V_{min} and V_{max}), their length, and their separation – also play a role, e.g. different learning responses are induced by small, rapid voltage pulses compared to large, infrequent pulses. This tunability provides flexibility to provide optimised memory effects for different computational tasks.

3 Discussion

3.1 Memristor ratio

We have focused here on PNNs in which 25% of the Type A gaps have been replaced with memristors. This allows us to focus on the correlated spiking dynamics in observed output signals (memristive hysteresis effects are present simultaneously, see e.g. Fig. 5f). We have studied networks with higher proportions of memristors and find similar hysteresis effects at low voltages (Fig. S2 (ESI†)), however as the number of spiking gaps decreases the number of observed spikes decreases. Thus the complexity of the spiking patterns is also reduced, and in the limit that all of the gaps are memristive (i.e. all the Type A gaps are replaced) there is no spiking. In this limit the continuous changes in outputs from the networks (see Fig. 3) are ideal for implementation of brain inspired algorithms based on reservoir computing.[25,26] Simulations of RC using networks of Type B and Type C memristors will be presented elsewhere.

In the biological brain, the ratio of synapses to neurons is on the order of 1000,[53] whereas in the simulated PNNs the ratio of Type B/C memristors (synapses) to Type A gaps (neurons) is much lower. The synapse to neuron ratio that can be achieved

in PNNs is limited by the mean degree (*i.e.* mean number of connections between nodes,[54] which is ~10). This is not necessarily an issue for the use of PNNs for computation – in fact, it is worth emphasising that the aim in the field of neuromorphic computing is to investigate what can be achieved with a *limited number* of brain-inspired elements rather than attempting to faithfully replicate all the details of the biological brain.

3.2 Experimental realisation

As mentioned in the introduction we believe that there are several possible routes to the addition of memristive synapses to spiking PNNs, including deposition of inorganic coating materials,[40] controlled sulphidisation of Ag or Cu PNNs,[6,41] and the introduction of novel memristive molecules.[42–44] We believe that the latter method is particularly promising, especially as a range of new molecular synapses are becoming available. Simple drop-casting methods should be sufficient to achieve mixed memristive/spiking networks, as it is usually straightforward to dilute the deposited solution in order to achieve a sparse random placement of molecules. The choice of molecule could also allow for precise selection of memristive properties, analogous to tuning the memristor parameters in the simulations described here. Of course it will be essential to build PNNs from non-reactive materials that can survive exposure to air, moisture and solvents.

4 Conclusion

We have shown that the addition of synapse-like memristive elements to the neuron-like spiking gaps that are inherently present in percolating networks of nanoparticles leads to significant changes in network dynamics. We highlight that the strengthening of Type B/C synaptic connections leads to increases in the connectivity between Type A neurons and consequently to increased neuronal spiking across the network. This results in biologically-realistic potentiation and de-potentiation of the networks in response to repeated input pulses, *i.e.* in learning and forgetting, which could be valuable for a variety of styles of neuromorphic computation.[30,37,47–49]

5 Methods

This section describes the basic features of the simulations. Note that a detailed comparison of the Type B and Type C memristor models is presented in Section S1 (ESI†).

5.1 Simulations

Results from experimental PNNs are well-described by continuum percolation models (see ref. 20 and references therein). Deposited particles are represented by disks that overlap after deposition, and overlapping disks form conducting nanoparticle groups. Deposition is ceased just before the 2D continuum percolation threshold (surface coverage $p < p_c \sim 0.68$)[23] is reached so that no single group fully spans the network, and

thus the network conductance results from tunnelling through gaps between the groups. We focus on networks with a surface coverage of $p = 0.65$ since this value is close enough to p_c to be near criticality but far enough away to ensure that unrealistic configurations (such as those dominated by very large groups) are avoided.[20] Similar results are obtained for $0.64 < p < p_c$.[21] The conductance of each gap is determined by its length L_i by

$$G_i = \alpha e^{-\beta L_i}, \qquad (1)$$

where $\alpha = 1\ \Omega^{-1}$ and $\beta = 200\ pd^{-1}$ are constants.[34] Note that the parameter β is in units of inverse particle diameters (pd^{-1}), and so the value of $\beta = 200\ pd^{-1}$ corresponds well with typical literature values[34,55] of ~10 nm^{-1} given experimental particle diameters of ~20 nm. The unit of length in the simulations is particle diameters and is thus normalised to 1.

When an external voltage stimulus is applied to the nano-particle groups chosen as the input electrodes, current flows through the network tunnel gaps as determined by Kirchhoff's laws.[20] The current that flows through the groups designated as the output electrodes is recorded.

5.2 Type A model

The formation and destruction of the atomic-scale filaments in *individual* Type A gaps is governed by a deterministic electric-field driven model.[20] The length of a growing filament d_i in gap i changes as a result of the local electric field E_i according to

$$\Delta d_i = \begin{cases} r_d(E_i - E_T), & E_i \geq E_T \\ 0, & \text{otherwise} \end{cases} \qquad (2)$$

and the width of each fully-formed filament w_i (which is initially w_0) thins due to its current I_i according to

$$\Delta w_i = \begin{cases} r_w(I_i - I_T), & I_i \geq I_T \\ 0, & \text{otherwise}, \end{cases} \qquad (3)$$

where E_T and I_T are the electric field and current thresholds required for filament formation and destruction, respectively, and r_d and r_w are the respective rates of formation and destruction. In the simulations $E_T = 10\ V\ pd^{-1}$ and $I_T = 0.01$ A, which are consistent with experimental estimates.[11] The conductance of a Type A gap depends on whether a filament had formed or not, *i.e.* it is either calculated based on its gap length L_i by eqn (1) if no filament is formed or it is set to $G_i = 10\ \Omega^{-1}$ if a filament is formed. The values of conductance parameters $G_{on} = 10\ \Omega^{-1}$ and $\alpha = 1\ \Omega^{-1}$ and constants E_T, I_T, r_d, and r_w could be scaled so that the magnitude of voltages, electric fields, and currents match experimental values more closely, but this does not change the overall results so we instead retain values that are consistent with previous work.[20,22]

r_d and r_w were tuned slightly for the 800×800 networks so that the spiking event rate match that of the 200×200 networks. The 800×800 networks were used to observe synaptic memory effects; see Section 2.6 and Section S4 (ESI†). This change increases the rate of Type A spiking which is necessary to match the spiking rates of smaller networks.

Table 1 Memristor parameters used for all simulations. The Type B parameter values are the same as those used in previous work,[24,25] except that $\alpha = 10$ Ω^{-1} was scaled to increase the conductance of the Type B memristors to increase their influence on the networks. The Type C parameter values were chosen to yield wide yet realistic hysteresis (see Fig. 3). See Section S1.4 (ESI) for detail on effect of varying α and G_{max}. Note that κ is dimensionless

Type B					Type C					
μ (nm^{-2} V^{-1})	κ	α (Ω^{-1})	β (pd^{-1})	T (s)	κ_{P0} (s^{-1})	κ_{D0} (s^{-1})	η_P (V^{-1})	η_D (V^{-1})	G_{min} (Ω^{-1})	G_{max} (Ω^{-1})
3.46×10^{-5}	3.8×10^{-2}	10	200	20	5×10^{-4}	5×10^{-2}	10	10	0	1

5.3 Type B model

The Type B model[25] governs the height of the partial hillocks that form in the tunnel gaps under an electric field. It is governed by the equation

$$\frac{dz}{dt} = \frac{1}{T}\left[\frac{\mu V}{D - z} - \kappa z\right], \tag{4}$$

where z is the hillock height, D is the total gap length, V is the gap potential, T is the characteristic time scale, and μ and κ are scaling parameters. This model has been shown to be equivalent to existing models of voltage-driven memristance,[24] and PNNs with tunnel gaps governed by this model in a low-voltage regime have been shown to perform well in RC tasks.[24,25] The characteristic time $T = 20$ s was chosen to tune the time scale of the Type B memristors to be comparable with that of the Type C memristors.

The conductance of memristor i is calculated by

$$G_i = \alpha e^{-\beta(D_i - z_i)}, \tag{5}$$

and so the current response to the gap voltage remains nonlinear, regardless of the linearity of the equation governing the hillock height z. See Table 1 for the parameters of the Type B model and Section S1.4 (ESI†) for detail on scaling the conductance parameter α.

In order to prevent numerical instabilities and unwanted spiking, the heights z were artificially limited to grow no larger than half of the gap lengths such that

$$0 \leq z_i \leq \frac{D_i}{2} \tag{6}$$

at all points of the simulation.

5.4 Type C model

The Type C model[8,39] is based on the rate-balance equation

$$\frac{dg}{dt} = \kappa_P(V)(1 - g) - \kappa_D(V)g, \tag{7}$$

where $0 \leq g \leq 1$ is the normalised conductance of the memristor. The parameters $\kappa_P(V)$ and $\kappa_D(V)$ are the potentiation and depression rate coefficients, respectively, and are functions of the local voltage such that

$$\kappa_P = \kappa_{P0}\exp(\eta_P V) \quad \& \quad \kappa_D = \kappa_{D0}\exp(-\eta_D V), \tag{8}$$

where $\kappa_{P0,D0}$ and $\eta_{P,D}$ are sub-parameters. The model[8] yields the exponential behaviour seen in electrochemical memristors.[50]

$$g_t = \frac{\kappa_P}{\kappa_P + \kappa_D}\left\{1 - \left[1 - \left(1 + \frac{\kappa_D}{\kappa_P}\right)g_{t-1}\right]e^{-(\kappa_P + \kappa_D)t}\right\} \tag{9}$$

for $t > 0$. The memristor conductance is then given by

$$G(t) = G_{min}(1 - g(t)) + G_{max}g(t), \tag{10}$$

where G_{min} and G_{max} are the minimum and maximum conductances of the memristor, respectively. The parameters of this model are listed in Table 1.

An advantage of the Type C model is its large number of parameters which allows for very fine control over the shape of the memristor hysteresis. Fig. S1 (ESI†) shows a range of examples of Type C hysteresis afforded by this model.

Author contributions

BM and ZH performed the simulations. BM, ZH and SAB performed data analysis. BM, ZH and SJS contributed to model development. ST, JG, FH and SAB conceptualised the project. BM and SAB wrote the first draft. All authors contributed to discussions and to writing the manuscript.

Conflicts of interest

There are no conflicts to declare.

Data availability

Data for this article are available *via* open science framework at **https://doi.org/10.17605/OSF.IO/49DKB**.

Acknowledgements

References

1 D. Marković, A. Mizrahi, D. Querlioz and J. Grollier, *Nat. Rev. Phys.*, 2020, **2**, 499–510.

2 A. Mehonic and A. J. Kenyon, *Nature*, 2022, **604**, 255–260.

3 V. Balasubramanian, *Proc. Natl. Acad. Sci. U. S. A.*, 2021, **118**, e2107022118.

4 Z. Kuncic and T. Nakayama, *Adv. Phys.:X*, 2021, **6**, 1894234.

5 A. Vahl, G. Milano, Z. Kuncic, S. A. Brown and P. Milani, *J. Phys. D: Appl. Phys.*, 2024, **57**, 503001.

6 A. Z. Stieg, A. V. Avizienis, H. O. Sillin, C. Martin-Olmos, M. Aono and J. K. Gimzewski, *Adv. Mater.*, 2012, **24**, 286–293.

7 J. Hochstetter, R. Zhu, A. Loeffler, A. Diaz-Alvarez, T. Nakayama and Z. Kuncic, *Nat. Commun.*, 2021, **12**, 4008.

8 G. Milano, G. Pedretti, K. Montano, S. Ricci, S. Hashemkhani, L. Boarino, D. Ielmini and C. Ricciardi, *Nat. Mater.*, 2022, **21**, 195–202.

9 H. Tanaka, S. Azhari, Y. Usami, D. Banerjee, T. Kotooka, O. Srikimkaew, T. T. Dang, S. Murazoe, R. Oyabu, K. Kimizuka and M. Hakoshima, *Neuromorphic Comput. Eng.*, 2022, **2**, 022002.

10 F. Caravelli, G. Milano, C. Ricciardi and Z. Kuncic, *Ann. Phys.*, 2023, **535**, 2300090.

11 A. Sattar, S. Fostner and S. A. Brown, *Phys. Rev. Lett.*, 2013, **111**, 136808.

12 S. K. Bose, J. B. Mallinson, R. M. Gazoni and S. A. Brown, *IEEE Trans. Electron Devices*, 2017, **64**, 5194–5201.

13 C. Minnai, A. Bellacicca, S. A. Brown and P. Milani, *Sci. Rep.*, 2017, **7**, 7955.

14 N. Carstens, T. Strunskus, F. Faupel, A. Hassanien and A. Vahl, *Part. Part. Syst. Charact.*, 2023, **40**, 2200131.

15 T. S. Rao, I. Mondal, B. Bannur and G. U. Kulkarni, *Discover Nano*, 2023, **18**, 124.

16 O. Gronenberg, B. Adejube, T. Hemke, J. Drewes, O. H. Asnaz, F. Ziegler, N. Carstens, T. Strunskus, U. Schürmann, J. Benedikt, T. Mussenbrock, F. Faupel, A. Vahl and L. Kienle, *Adv. Funct. Mater.*, 2024, **34**, 2312989.

17 A. J. T. V. D. Ree, M. Ahmadi, G. H. T. Brink, B. J. Kooi and G. Palasantzas, *Phys. Rev. Mater.*, 2025, **9**, 036001.

18 M. Davies, N. Srinivasa, T.-H. Lin, G. Chinya, Y. Cao, H. Choday, G. Dimou, P. Joshi, N. Imam, S. Jain, Y. Liao, C.-K. Lin, A. Lines, R. Liu, D. Mathaikutty, S. Mccoy, A. Paul, J. Tse, G. Venkataramanan, Y.-H. Weng, A. Wild, Y. Yang and H. Wang, *IEEE Micro*, 2018, **38**, 82–99.

19 J. B. Mallinson, S. Shirai, S. K. Acharya, S. K. Bose, E. Galli and S. A. Brown, *Sci. Adv.*, 2019, **5**, eaaw8438.

20 M. D. Pike, S. K. Bose, J. B. Mallinson, S. K. Acharya, S. Shirai, E. Galli, S. J. Weddell, P. J. Bones, M. D. Arnold and S. A. Brown, *Nano Lett.*, 2020, **20**, 3935–3942.

21 S. Shirai, S. K. Acharya, S. K. Bose, J. B. Mallinson, E. Galli, M. D. Pike, M. D. Arnold and S. A. Brown, *Network Neurosci.*, 2020, **4**, 432–447.

22 S. K. Acharya, E. Galli, J. B. Mallinson, S. K. Bose, F. Wagner, Z. E. Heywood, P. J. Bones, M. D. Arnold and S. A. Brown, *ACS Appl. Mater. Interfaces*, 2021, **13**, 52861–52870.

23 D. Stauffer and A. Aharony, *Introduction to Percolation Theory*, Taylor and Francis, 2nd edn, 1994.

24 R. K. Daniels, J. B. Mallinson, Z. E. Heywood, P. J. Bones, M. D. Arnold and S. A. Brown, *Neural Networks*, 2022, **154**, 122–130.

25 J. B. Mallinson, Z. E. Heywood, R. K. Daniels, M. D. Arnold, P. J. Bones and S. A. Brown, *Nanoscale*, 2023, **15**, 9663–9674.

26 J. B. Mallinson, J. K. Steel, Z. E. Heywood, S. J. Studholme, P. J. Bones and S. A. Brown, *Adv. Mater.*, 2024, **36**, 2402319.

27 Z. E. Heywood, J. B. Mallinson, P. J. Bones and S. A. Brown, *Neuromorphic Comput. Eng.*, 2024, **4**, 034011.

28 Z. E. Heywood, B. L. Monaghan, J. B. Mallinson and S. A. Brown, 2025, submitted.

29 S. J. Studholme, Z. E. Heywood, J. B. Mallinson, J. K. Steel, P. J. Bones, M. D. Arnold and S. A. Brown, *Nano Lett.*, 2023, **23**, 10594–10599.

30 S. J. Studholme, J. B. Mallinson, J. K. Steel and S. A. Brown, *Neuromorphic Comput. Eng.*, 2025, **5**, 014017.

31 W. L. Shew and D. Plenz, *Neuroscientist*, 2013, **19**, 88–100.

32 J. O'Byrne and K. Jerbi, *Trends Neurosci.*, 2022, **45**, 820–837.

33 S. J. Studholme and S. A. Brown, *ACS Nano*, 2024, **18**, 28060–28069.

34 S. Fostner, R. Brown, J. Carr and S. A. Brown, *Phys. Rev. B:Condens. Matter Mater. Phys.*, 2014, **89**, 075402.

35 T. Takeuchi, A. J. Duszkiewicz and R. G. Morris, *Philos. Trans. R. Soc., B*, 2014, **369**, 20130288.

36 H. G. Manning, F. Niosi, C. G. da Rocha, A. T. Bellew, C. OCallaghan, S. Biswas, P. F. Flowers, B. J. Wiley, J. D. Holmes, M. S. Ferreira and J. J. Boland, *Nat. Commun.*, 2018, **9**, 3219.

37 W. Wang, G. Pedretti, V. Milo, R. Carboni, A. Calderoni, N. Ramaswamy, A. S. Spinelli and D. Ielmini, *Sci. Adv.*, 2018, **4**, eaat4752.

38 G. Milano, K. Montano and C. Ricciardi, *J. Phys. D: Appl. Phys.*, 2023, **56**, 084005.

39 E. Miranda, G. Milano and C. Ricciardi, *IEEE Trans. Nanotechnol.*, 2020, **19**, 609–612.

40 N. Carstens, B. Adejube, T. Strunskus, F. Faupel, S. Brown and A. Vahl, *Nanoscale Adv.*, 2022, **4**, 3149–3160.

41 Z. Xu, Y. Bando, W. Wang, X. Bai and D. Golberg, *ACS Nano*, 2010, **4**, 2515–2522.

42 Y. Wang, Q. Zhang, H. P. Astier, C. Nickle, S. Soni, F. A. Alami, A. Borrini, Z. Zhang, C. Honnigfort, B. Braunschweig, A. Leoncini, D. C. Qi, Y. Han, E. del Barco, D. Thompson and C. A. Nijhuis, *Nat. Mater.*, 2022, **21**, 1403–1411.

43 Y. Zhang, L. Liu, B. Tu, B. Cui, J. Guo, X. Zhao, J. Wang and Y. Yan, *Nat. Commun.*, 2023, **14**, 247.

44 R. S. Williams, S. Goswami and S. Goswami, *Nat. Mater.*, 2024, **23**, 1475–1485.

45 C. Huez, D. Guérin, F. Volatron, A. Proust and D. Vuillaume, *Nanoscale*, 2024, **16**, 21571–21581.

46 R. L. Davis and Y. Zhong, *Neuron*, 2017, **95**, 490–503.

47 S. Wu, K. Y. M. Wong and M. Tsodyks, *Front. Comput. Neurosci.*, 2013, **7**, 188.

48 S. Lim, J. L. McKee, L. Woloszyn, Y. Amit, D. J. Freedman, D. L. Sheinberg and N. Brunel, *Nat. Neurosci.*, 2015, **18**, 1804–1810.

49 B. Voloh, M. Oemisch and T. Womelsdorf, *Nat. Commun.*, 2020, **11**, 4669.

50 I. Valov, R. Waser, J. R. Jameson and M. N. Kozicki, *Nanotechnology*, 2011, **22**, 254003.

51 L. J. Fosque, R. V. Williams-García, J. M. Beggs and G. Ortiz, *Phys. Rev. Lett.*, 2021, **126**, 098101.

52 A. Citri and R. C. Malenka, *Neuropsychopharmacology*, 2008, **33**, 18–41.

53 S. Budday, P. Steinmann and E. Kuhl, *Front. Cell. Neurosci.*, 2015, **9**, 257.

54 R. K. Daniels, M. D. Arnold, Z. E. Heywood, J. B. Mallinson, P. J. Bones and S. A. Brown, *Phys. Rev. Appl.*, 2023, **20**, 034021.

55 H. Moreira, J. Grisolia, N. M. Sangeetha, N. Decorde, C. Farcau, B. Viallet, K. Chen, G. Viau and L. Ressier, *Nanotechnology*, 2013, **24**, 095701.